Supporting Information

Fichou et al. 10.1073/pnas.1422824112

SI Materials and Methods

Expression and Purification of Unlabeled and Perdeuterated htau40 Protein. The protocol for expression and purification of the human isoform htau40 has been published elsewhere (1). Briefly, the protein was expressed as a histidine-tagged fusion protein in *Escherichia coli* BL21(DE3). To produce hydrogenated protein, the bacteria grew in LB medium in 2-L flasks. The induction of protein expression was done by adding isopropyl-β-D-thiogalactoside (IPTG) to a final concentration of 0.5 mM, once the optical density at 600 nm (OD_{600}) reached 0.8. The bacteria were harvested after 3 h of incubation at 30 °C.

To obtain perdeuterated protein, a high-cell-density fermentation process with deuterated Enfors minimal medium was used to grow bacteria to an OD_{600} of 12–14, followed by induction of protein expression by IPTG to a final concentration of 0.5 mM. D8-glycerol (fully deuterated glycerol) was used as the carbon source, and D_2O was used as the solvent. Bacteria were harvested when an OD_{600} of 20 was reached.

The expressed protein was purified by immobilized metal ion affinity chromatography on a nickel affinity column, followed by size-exclusion chromatography. All purification steps were conducted in H_2O-based buffer systems. Protein purity was assessed by 14% Tris-Tricine SDS/PAGE.

Production of Deuterated Heparin Analog. *E. coli* K5 bacteria were grown in Enfors deuterated medium and perdeuterated heparosan (N-acetyl-glucosamine-glucuronic acid repeats) polysaccharides were isolated as described in ref. 2. Chemical modifications were adapted from Casu et al. (3) to produce poly N- and O-sulfated heparosans. Heparosan at 0.5 mg/mL was deacetylated in 2 M NaOH for 16 h at 56 °C. The pH was adjusted to 7.5, and polysaccharides were extensively dialyzed against water and freeze dried. N-sulfation was achieved by addition to N-deacetylated heparosan of 30 mg/mL pyridine-sulfotrioxyde and Na_2CO_3 at 1.5 mg/mL in water for 16 h at 56 °C. The same amounts of pyridine-sulfotrioxyde and Na_2CO_3 were again added and further incubated for 8 h. For O-sulfation, the above described materials (N-sulfated heparosans) were dialyzed against water and run through an Amberlite IR120 column at 4 °C. The pH was adjusted to 5.5 with 10% tributylamine (TBA), and the heparosans were freeze dried. N-sulfated heparosans (TBA form) were dissolved in dimethylsulfoxyde at 3 mg/mL with 200 mg/mL pyridine-sulfotrioxyde for 2 h at 25 °C. The O-sulfation reaction was stopped by a two-times dilution in water, and pH was adjusted to 8 with NaOH. O-sulfated heparosans were precipitated with 80% NaCl-saturated acetone at −20 °C and washed in NaCl-saturated acetone, and the final pellet was dried and resuspended in 0.2 M NaCl. A final N-sulfation step was then performed before extensively dialyzing the polysaccharides against water.

Tau Fiber Formation and Monitoring. See *Materials and Methods* for details.

Sample Preparation for Neutron Scattering Experiments. After centrifugation, the pellet was lyophilized and dried over P_2O_5 for 4 d on a 4 × 3 cm^2 flat aluminum sample holder. Dolman et al. (4) reported that after such a procedure, lysozyme retains only four tightly bound structural water molecules. The resulting hydration level was defined as 0 g water per gram of tau.

The deuterated fibers (106 mg of dry protein) were rehydrated to 0.40 g H_2O per gram of protein (sample referred to as D-fiber-H_2O). The hydrogenated fibers (116 mg of dry protein) were first kept for 17 h under 100% D_2O atmosphere and then dried over P_2O_5 until they reached a hydration level of 0.44 g D_2O per gram of protein (sample denoted as H-fiber-D_2O). Both samples were then sealed by an aluminum cover (0.3-mm neutron path length) and an indium seal with a diameter of 1 mm.

The deuterated and hydrogenated monomeric protein samples (D-tau-H_2O and H-tau-D_2O) had been prepared earlier (1). We recall that the hydration level was 0.38 g H_2O per gram of protein and 0.44 g D_2O per gram of protein for D-tau-H_2O and H-tau-D_2O, respectively. They were reused for the present work without opening the sample holders.

If we assume that all exchangeable hydrogen/deuterium atoms (i.e., 24% of all hydrogen/deuterons in the protein) exchange, the following contributions to the total incoherent scattering cross section of the samples are obtained by summing individual incoherent scattering cross sections of the constituting atoms: (*i*) for D-tau-H_2O and D-fiber-H_2O samples, 71% from hydration water (H_2O) and 29% from protein (8% from the deuterated protein and 92% from the deuterons exchanged against hydrogens) and (*ii*) for H-tau-D_2O and H-fiber-D_2O samples, 97% protein (99% from hydrogenated protein and 1% from the hydrogen atoms exchanged against deuterons) and 3% from hydration water (D_2O).

Several studies on tau fibrillation triggered by heparin showed that only a small amount of heparin, if any, is found in the mature fibers (5–8). As an additional precaution, we used deuterated heparin so that, even if the ratio tau:heparin was 1:1 in the mature fibers, the heparin contribution to the total scattering intensity in both fiber samples would be less that 0.5%. Thus, the contribution of heparin in the above calculations was neglected.

Fiber Characterization by Electron Microscopy and X-Ray Diffraction.
Electron microscopy. The samples were negatively stained using the mica floatation technique. Then 4 μl of the protein sample were adsorbed onto the clean side of a carbon film on a mica sheet (carbon/mica interface) and, after 30 s, negatively stained with 2% (wt/vol) uranyl acetate (pH 4.5). Micrographs were taken under low-dose conditions with a CM12 LaB6 electron microscope working at 120 kV and with nominal magnifications of 22,000× and 45,000× using a Gatan OriusTM SC1000 CCD camera. The micrograph of the D-fiber sample is shown in Fig. 2*A*, and we show in Fig. S1*A* the micrograph of the H-fiber sample. As a control, we also monitored the protein before adding heparin, and no fibers were visible (not shown).

X-ray diffraction. The experiments were performed at the European Synchrotron Radiation Facility Synchrotron (Grenoble, France) on beamlines ID14-1 and ID23-2 for the hydrogenated and deuterated fibers, respectively. Hydrogenated fibers were mounted after lyophilization into a nylon loop of 0.5 mm diameter. The sample was then exposed to a monochromatic X-ray beam of 0.93 Å wavelength during 100 s at room temperature, while the sample was rotated by a total of 1 degree. For the deuterated fibers, a drop of fiber solution was dried out between two thin glass capillaries. The dry residue was then exposed to a monochromatic beam of 0.87 Å wavelength during 10 s at room temperature. The diffraction pattern of the deuterated fibers is shown in Fig. 2*B*, and the one of hydrogenated fibers is shown in Fig. S1*B*.

EINS Experiments.
Deuterated samples (D-tau-H_2O and D-fiber-H_2O). EINS experiments were carried out on the backscattering spectrometer SPHERES

(Jülich Centre for Neutron Science at the Heinz Maier-Leibnitz-Zentrum Garching, Garching, Germany). Each sample was inserted at room temperature into a Janis cryostat at 135° with respect to the incoming neutron beam. The temperature was lowered to 20 K during about 2 h. Elastically scattered neutrons were then counted while the temperature was continuously increased from 20 K to 300 K at a rate of 0.093 K/min for D-fiber-H_2O and of 0.156 K/min for D-tau-H_2O.

The elastically scattered intensity of the samples were then calculated according to the following formula:

$$I_{sample,T}(q) = \frac{I_{total,T}(q) - tr \times I_{empty}(q)}{\langle I_{total,T}(q) - tr \times I_{empty}(q) \rangle_{20-40\ \mathrm{K}}} \qquad \textbf{[S1]}$$

where $I_{sample,T}(q)$ is the normalized intensity scattered from the sample at the temperature T, corrected for instrument effects and empty cell scattering; $I_{total,T}(q)$ is the measured intensity; and $I_{empty}(q)$ is the scattered intensity from an empty cell measured at 280 K. The brackets represent the elastic intensity averaged in the temperature window 20–40 K, and tr is the measured sample transmission.

Because the more dynamic the system is, the less neutrons are elastically scattered, one can sum the elastic intensity over all q values to obtain a qualitative model-free information about the dynamics of the system, as shown in Fig. S2. More quantitatively, the atomic mean square displacements (MSD, $\langle u^2 \rangle$) were extracted from the q dependence of the elastic intensity that can be described in the Gaussian approximation by

$$I_{sample,T}(q) = \exp\left(\frac{-q^2\langle u^2 \rangle}{6}\right). \qquad \textbf{[S2]}$$

MSD were extracted in the q range where the logarithm of the elastic intensity remains linear with respect to q^2, i.e., 0.78 $Å^{-1}$ < q < 1.76 $Å^{-1}$ for both D-tau-H_2O and D-fiber-H_2O samples.

Hydrogenated samples (H-tau-D_2O and H-fiber-D_2O). EINS experiments were carried out on the backscattering spectrometer IN16 at the Institut Laue Langevin (ILL; Grenoble, France). The H-fiber-D_2O sample was inserted at room temperature into an orange ILL cryostat at 135° with respect to the incoming neutron beam. The temperature was lowered to 20 K over 2 h. Elastically scattered neutrons were then counted while the temperature was continuously increased from 20 K to 300 K at a rate of 0.14 K/min. The elastically scattered signals were then processed according to Eq. **S1**. Data on H-tau-D_2O, measured on IN16 according to the same protocol, were taken from previous work (1) and reprocessed. At high q values, the deviation from the Gaussian approximation expressed in Eq. **S2** is nonnegligible. Such a deviation can have two different origins: non-Gaussian scattering from single atoms and dynamic heterogeneity. A simple correction with a q^4 term has been proposed (9, 10), in which the scattering intensity can be expressed as follows:

$$I_{sample,T}(q) = \exp\left(\frac{-q^2\langle u^2 \rangle}{6}\right) \times \left(1 + \frac{q^2}{72}\sigma^2\right) \qquad \textbf{[S3]}$$

where σ^2 is the variance of the distribution of the MSD, if we assume that the dynamical heterogeneity is the main contribution to the non-Gaussian behavior. An example of the fit from the Gaussian approximation with and without q^4 correction is shown in Fig. S4. This model allows extracting the MSD (see Fig. 3*C*) as well as the MSD variance shown in Fig. S5, which reflects the MSD heterogeneity among hydrogen atoms in the sample. These two parameters were extracted by fitting Eq. **S3** between the q values 0.43 $Å^{-1}$ and 1.93 $Å^{-1}$ for both H-tau-D_2O and H-fiber-D_2O samples.

QENS. The model used and the fitting procedure have been extensively discussed in a recent study (11). Briefly we used a rotational–translational diffusion model, where each water molecule is considered to either undergo rotational or translational diffusion, or to be immobile. We used a global fitting approach where all spectra were simultaneously fitted at all q values with the following equation:

$$S(q,\omega) = DW(q)[[A_0 \times \delta(\omega) + A_t \times S_t(q,\omega) + A_r \times S_r(q,\omega)] \otimes R(q,\omega) + k(q)] \qquad \textbf{[S4]}$$

where $DW(q) = \exp(-q^2\langle u^2 \rangle)$ is the Debye–Waller factor due to the vibrational motions. The intensity of the elastic term [$A_0 = A_r \cdot J_0^2(qb) + A_i$, where J_0 is the 0th order spherical Bessel function] contains a q-dependent term from the rotational diffusion model and a q-independent term A_i that takes into account hydrogen atoms not moving in the timescale set by the resolution function. $S_t(q,\omega) \propto \frac{Dq^\lambda}{\omega^2 + (Dq^\lambda)^2}$ is the contribution of translational motions; for $\lambda = 2$, the standard Brownian diffusion is recovered, whereas $\lambda < 2$ indicates a subdiffusive character, often found in polymers and glass-forming and supercooled liquids.

$S_r(q,\omega) \propto \sum_{l=1}(2l+1)J_l^2(qb)\frac{1}{\pi}\frac{l(l+1)\Gamma}{\omega^2 + (l(l+1)\Gamma)^2}$ is the contribution to the quasi-elastic broadening of rotational motions ; b is the radius of the hydrogen rotation around the center of mass of water molecule, that was set to 0.98 Å, i.e., the H–O distance (the center of mass position essentially coincides with the oxygen atom position); $J_l(qb)$ are the spherical Bessel functions. The free parameters are in this model are then $\langle u^2 \rangle$, A_i, A_t, D, λ, A_r, Γ, and $k(q)$ for a complete dataset at a given temperature.

MD Simulations. The MD simulations were performed with the NAMD program (12) using the CHARMM27 force field (13, 14) for the protein and the TIP3P model (15) for water. The simulations were maintained at constant temperature using Langevin dynamics, and at a constant pressure of 1 atm using the Nosé–Hoover Langevin piston algorithm with anisotropic cell fluctuations (16, 17). The equations of motion were integrated using the Verlet-I/r-RESPA multiple time step algorithm (18, 19) with time steps of 2 fs for the long-range nonbonded forces, 2 fs for the short-range nonbonded forces, and 2 fs for the bonded intramolecular forces. The SHAKE algorithm (20) was used to constrain the lengths of all bonds to H atoms. Electrostatic interactions were computed using the smooth particle mesh Ewald sum (21), and the van der Waals interactions and the real space part of the Ewald sum were smoothly switched to zero over the range 10–12 Å.

The monomeric peptide model was built by placing the hexapeptide VQIVYK in a box containing 9,253 water molecules and 1 chloride ion (see the snapshot in Fig. S6*A*). An energy minimization was carried out for 20 ps before equilibrating the system for 12 ns. The fiber model was based on the work of Zhao et al. (22). The fiber was made of the antiparallel two-sheet crystal structure published by Sawaya et al. (23) (PDB entry 2ON9). Five strands were stacked on each other with a spacing distance of 4.7 Å as shown in Fig. S6*B*. The fiber backbone was first harmonically constrained and placed in a box with 10 chloride ions for 10 ns. The system was then equilibrated with 9,258 water molecules for 4 ns with the same harmonic constraints. Finally, the system was equilibrated without constraints for 18 ns.

The time correlation functions shown in Fig. 4 were computed over a 2-ns-long trajectory saved every 0.1 ps for water molecules within 3 Å of the protein (see Fig. S6). For a rigorous comparison, only the water molecules around one central peptide of the fiber were considered (see Fig. S6*B*). The intermittent HB relaxation is described by the decay of the correlation function $c(t) = \langle h(0)h(t) \rangle / \langle h \rangle$ (24), where $h(t)$ is an HB population operator,

which is equal to 1 if a given donor–acceptor (D–A) pair is hydrogen bonded at time t, and zero otherwise, and the angular brackets denote an average over all D–A pairs (Fig. 4*C*). The function c(t) is the probability that a random D–A pair that is hydrogen bonded at time 0 is still bonded at time t, regardless of whether or not the bond was broken at intermediate times. The timescale of the decay of the continuous HB relaxation time represents the lifetime of protein–water HBs that are formed/broken by water rotational/librational motions on the protein surface (Fig. 4*B*).

1. Gallat F-X, et al. (2012) Dynamical coupling of intrinsically disordered proteins and their hydration water: Comparison with folded soluble and membrane proteins. *Biophys J* 103(1):129–136.
2. Laguri C, et al. (2011) ^{13}C-labeled heparan sulfate analogue as a tool to study protein/heparan sulfate interactions by NMR spectroscopy: Application to the CXCL12α chemokine. *J Am Chem Soc* 133(25):9642–9645.
3. Casu B, et al. (1994) Heparin-like compounds prepared by chemical modification of capsular polysaccharide from *E. coli* K5. *Carbohydr Res* 263(2):271–284.
4. Dolman M, Halling PJ, Moore BD, Waldron S (1997) How dry are anhydrous enzymes? Measurement of residual and buried ^{18}O-labeled water molecules using mass spectrometry. *Biopolymers* 41(3):313–321.
5. von Bergen M, et al. (2006) The core of tau-paired helical filaments studied by scanning transmission electron microscopy and limited proteolysis. *Biochemistry* 45(20):6446–6457.
6. Sibille N, et al. (2006) Structural impact of heparin binding to full-length Tau as studied by NMR spectroscopy. *Biochemistry* 45(41):12560–12572.
7. Carlson SW, et al. (2007) A complex mechanism for inducer mediated tau polymerization. *Biochemistry* 46(30):8838–8849.
8. Ramachandran G, Udgaonkar JB (2011) Understanding the kinetic roles of the inducer heparin and of rod-like protofibrils during amyloid fibril formation by Tau protein. *J Biol Chem* 286(45):38948–38959.
9. Becker T, Smith JC (2003) Energy resolution and dynamical heterogeneity effects on elastic incoherent neutron scattering from molecular systems. *Phys Rev E Stat Nonlin Soft Matter Phys* 67(2 Pt 1):021904.
10. Yi Z, Miao Y, Baudry J, Jain N, Smith JC (2012) Derivation of mean-square displacements for protein dynamics from elastic incoherent neutron scattering. *J Phys Chem B* 116(16):5028–5036.
11. Schiró G, et al. (2015) Translational diffusion of hydration water correlates with functional motions in folded and intrinsically disordered proteins, *Nat Commun* 6:6490.
12. Phillips JC, et al. (2005) Scalable molecular dynamics with NAMD. *J Comput Chem* 26(16):1781–1802.
13. MacKerell AD, et al. (1998) All-atom empirical potential for molecular modeling and dynamics studies of proteins. *J Phys Chem B* 102(18):3586–3616.
14. Mackerell AD, Jr, Feig M, Brooks CL, 3rd (2004) Extending the treatment of backbone energetics in protein force fields: Limitations of gas-phase quantum mechanics in reproducing protein conformational distributions in molecular dynamics simulations. *J Comput Chem* 25(11):1400–1415.
15. Jorgensen WL, Chandrasekhar J, Madura JD, Impey RW, Klein ML (1983) Comparison of simple potential functions for simulating liquid water. *J Chem Phys* 79(2):926–935.
16. Martyna GJ, Tobias DJ, Klein ML (1994) Constant pressure molecular dynamics algorithms. *J Chem Phys* 101(5):4177–4189.
17. Feller SE, Zhang Y, Pastor RW, Brooks BR (1995) Constant pressure molecular dynamics simulation: The Langevin piston method. *J Chem Phys* 103(11):4613–4621.
18. Grubmüller H, Heller H, Windemuth A, Schulten K (1991) Generalized Verlet algorithm for efficient molecular dynamics simulations with long-range interactions. *Mol Simul* 6(1-3):121–142.
19. Tuckerman M, Berne BJ, Martyna GJ (1992) Reversible multiple time scale molecular dynamics. *J Chem Phys* 97(3):1990–2001.
20. Ryckaert J-P, Ciccotti G, Berendsen HJC (1977) Numerical integration of the Cartesian equations of motion of a system with constraints: Molecular dynamics of n-alkanes. *J Comput Phys* 23(3):327–341.
21. Essmann U, et al. (1995) A smooth particle mesh Ewald method. *J Chem Phys* 103(19):8577–8593.
22. Zhao J-H, et al. (2010) Molecular dynamics simulations to investigate the stability and aggregation behaviour of the amyloid-forming peptide VQIVYK from tau protein. *Mol Simul* 36(13):1013–1024.
23. Sawaya MR, et al. (2007) Atomic structures of amyloid cross-β spines reveal varied steric zippers. *Nature* 447(7143):453–457.
24. Luzar A, Chandler D (1996) Effect of environment on hydrogen bond dynamics in liquid water. *Phys Rev Lett* 76(6):928–931.

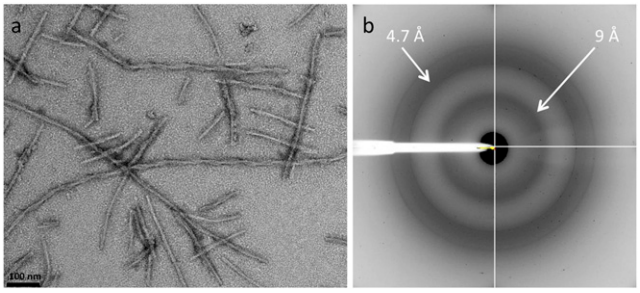

Fig. S1. (*A*) Electron micrograph and (*B*) X-ray fiber diffraction pattern of hydrogenated tau amyloid fibers (H-fiber).

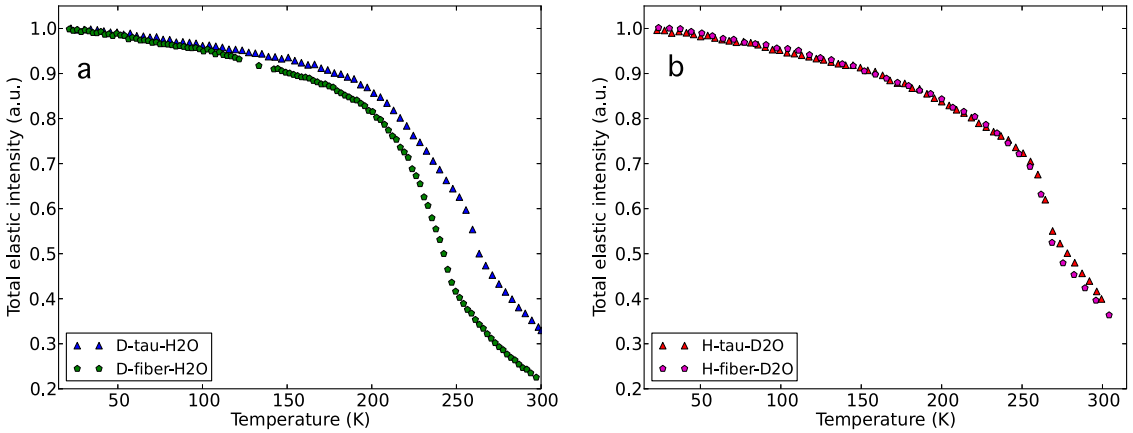

Fig. S2. Total elastic intensities integrated over all detectors for (*A*) D-tau-H_2O and D-fiber-H_2O (q range is 0.21–1.84 Å^{-1}) and (*B*) H-tau-D_2O and H-fiber-D_2O (q range is 0.19–1.95 Å^{-1}). Data from H-tau-D_2O were taken from ref. 1.

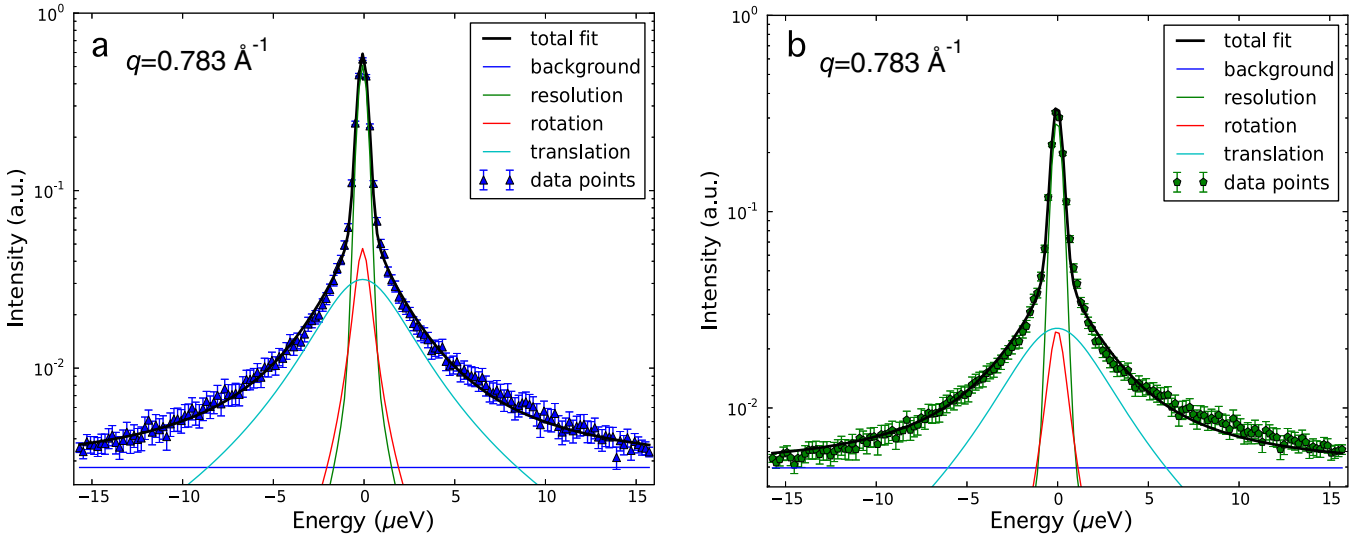

Fig. S3. QENS spectra of (*A*) D-fiber-H_2O and (*B*) D-tau-H_2O at $q = 0.78$ Å^{-1} and the corresponding fit from the translational–rotational model. Data on D-tau-H_2O were extracted from previous work (11).

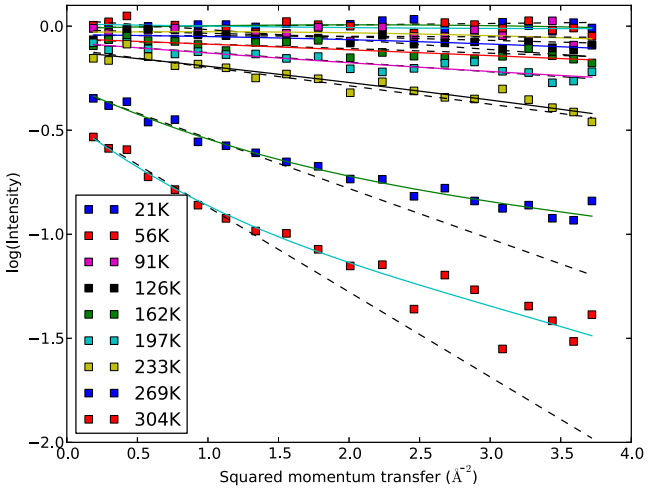

Fig. S4. Example of fits from the Gaussian approximation (dashed lines) and the q^4 correction model (continuous lines) applied on the tau amyloid fibers (H-fiber-D_2O).

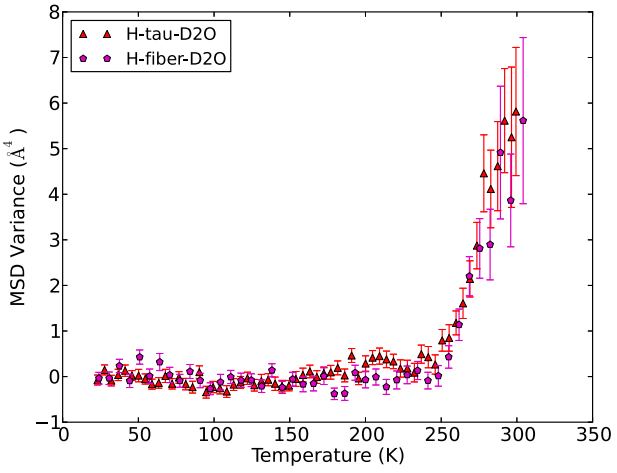

Fig. S5. MSD variance obtained from q^4 correction model (Eq. **S3**).

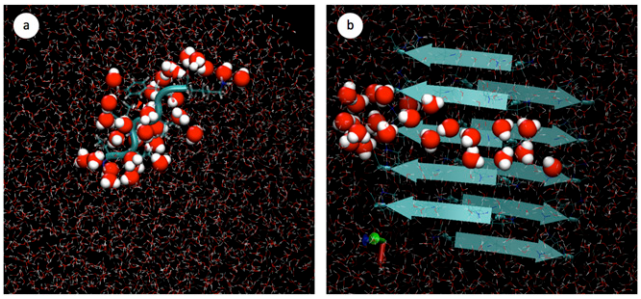

Fig. S6. Snapshots of the simulation box of the amyloidogenic peptide ^{306}VQIVYK^{311} (*A*) as monomer in solution and (*B*) in an amyloid assembly constructed from the crystal structure of PDB entry 2ON9. The analyzed water molecules are depicted with spheres with van der Waals radii.

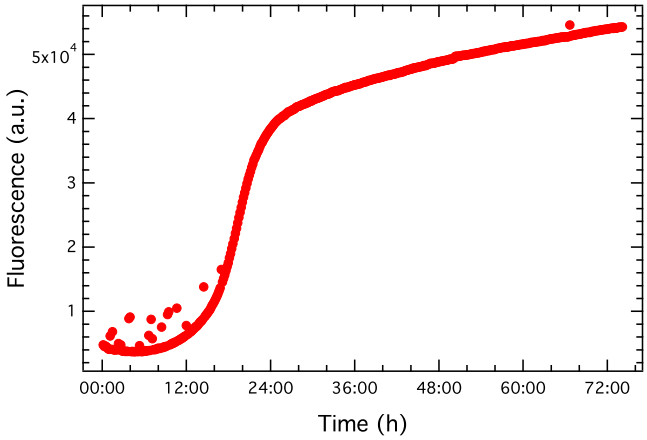

Fig. S7. Fluorescence of thioflavin S that was added to the hydrogenated protein mixed with deuterated heparin; $t = 0$ denotes the time point when heparin is added to the protein solution. The solution was excited at 430 nm, and the emission was measured at 490 nm.

Table S1. Fitting parameters of the QENS spectra of D-fiber-H_2O and D-tau-H_2O at 280 K

	D-tau-H_2O	D-fiber-H_2O	Change from D-tau-H_2O to D-fiber-H_2O, %
Immobile fraction	0.04 ± 0.02	0.04 ± 0.03	0
Translational fraction	0.381 ± 0.005	0.475 ± 0.008	+25
Trans. diff. coeff., 10^{-7} cm^2/s	0.99 ± 0.03	1.10 ± 0.04	+11
Rotational fraction	0.58 ± 0.03	0.49 ± 0.03	−16
Rotational rate, ps^{-1}	58 ± 9	68 ± 5	+17
λ	1.80 ± 0.07	1.80 ± 0.08	0

The errors represent SD output from the fitting procedure. An example of the fit is shown in Fig. S3. The final column shows the relative change of the parameters between the two samples. Trans. diff. coeff., translational diffusion coefficient.